Supplementary Materials

In this Supplementary Information, we provide a detailed exposition of the analysis presented in the main text. We derive corresponding rate equations from stochastic models based on a mean-field assumption and identify the equilibrium triad frequencies analytically under certain parameter conditions. We also present numerical results to complement our analysis.

CONTENTS

1. Rate equations 2

2. Equilibrium triad frequencies 7

3. Focal-link model: approximate steady-state solution 8
   3.1. Approximate equilibrium frequency of Δ_1 triads 8
   3.2. Derivation of an approximate expression for r_1 using a power-series expansion 8
   3.3. Approximate equilibrium frequencies of Δ_3 and Δ_6 triads 9

4. Focal-triad model: approximate steady-state solution 11
   4.1. Approximate equilibrium frequency of Δ_1 triads 11
   4.2. Derivation of an approximate expression for r_1 using an asymptotic expansion 11
   4.3. Approximate equilibrium frequencies of Δ_3 and Δ_6 triads 12

5. Frequency of irrational updates 14

6. Time-series triad frequencies with fully polarized initial states 15

1. RATE EQUATIONS

Let $L = \binom{N}{2}$ and $N_\Delta = \binom{N}{3}$ denote the total numbers of links and triads in the network, respectively. We represent the numbers of positive, negative, and neutral links by L^σ, where $\sigma \in \{+1, -1, 0\}$, respectively. There are ten types of triads up to permutation. We denote them by Δ_k ($k = 0, \cdots, 9$) as illustrated in Figure 1 in the main text. We also represent the number of type-k triads by N_k. The normalization constraint requires that $L = \sum_\sigma L^\sigma$ and $N_\Delta = \sum_k N_k$. We define these quantities in density form as well: $\rho^\sigma = L^\sigma/L$, $n_k = N_k/N_\Delta$. The key quantity to work with is the average number of triads of type k that involves a link σ, which we denote by N_k^σ. For convenience, we also define $n_k^\sigma = N_k^\sigma/(N-2)$. We refer the reader to Table S1 for a list of symbols and notations.

It follows from the definition that

$$
\begin{aligned}
L^0 &= \frac{3N_0 + 2N_1 + 2N_2 + N_3 + N_4 + N_5}{N-2}, \\
L^+ &= \frac{N_1 + 2N_3 + N_4 + 3N_6 + 2N_7 + N_8}{N-2}, \\
L^- &= \frac{N_2 + N_4 + 2N_5 + N_7 + 2N_8 + 3N_9}{N-2}.
\end{aligned}
$$

Therefore, the densities of neutral, positive, and negative links are given by

$$
\rho^0 = \frac{m^0}{3}, \quad \rho^+ = \frac{m^+}{3}, \quad \rho^- = \frac{m^-}{3},
$$

where we have defined

$$
\begin{aligned}
m^0 &= 3n_0 + 2n_1 + 2n_2 + n_3 + n_4 + n_5, \\
m^+ &= n_1 + 2n_3 + n_4 + 3n_6 + 2n_7 + n_8, \\
m^- &= n_2 + n_4 + 2n_5 + n_7 + 2n_8 + 3n_9.
\end{aligned}
$$

Table S1. Description of the symbols and notations used in our mean-field analysis.

Symbol	Description
L	Total number of links
N_Δ	Total number of triads
L^σ	Number of either positive, negative, or neutral links ($\sigma \in \{1, -1, 0\}$)
Δ_k	Triad type k
N_k	Number of type-k triads
ρ^σ	Frequency of σ-links ($\rho^\sigma = L^\sigma/L$)
n_k	Frequency of type-k triads ($n_k = N_k/N_\Delta$)
N_k^σ	Average number of type-k triads that are attached to a link σ
n_k^σ	Average density of type-k triads that are attached to a link σ ($n_k^\sigma = N_k^\sigma/(N-2)$)
$p_\sigma^{\sigma'}$	Probability that a link changes its sign from σ to σ'

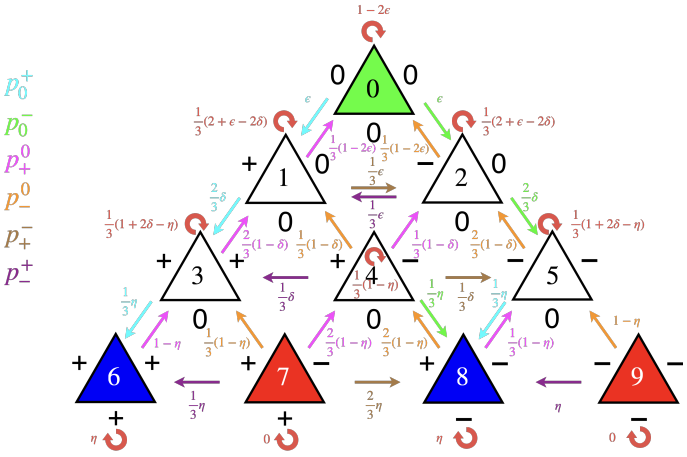

Figure S1. Illustration of the probabilities of transition between different triad types in the focal-link model, derived from the model definition. The probabilities $\{p_\sigma^{\sigma'}\}_{\sigma\neq\sigma'}$ are obtained by summing all terms of the same color associated with the corresponding arrows.

Then, we find

$$
\begin{aligned}
n_0^0 &= \frac{3n_0}{m^0}, \\
n_1^0 &= \frac{2n_1}{m^0}, \quad n_1^+ = \frac{n_1}{m^+}, \\
n_2^0 &= \frac{2n_2}{m^0}, \quad n_2^- = \frac{n_2}{m^-}, \\
n_3^0 &= \frac{n_3}{m^0}, \quad n_3^+ = \frac{2n_3}{m^+}, \\
n_4^0 &= \frac{n_4}{m^0}, \quad n_4^+ = \frac{n_4}{m^+}, \quad n_4^- = \frac{n_4}{m^-}, \\
n_5^0 &= \frac{n_5}{m^0}, \quad n_5^- = \frac{2n_5}{m^-}, \\
n_6^+ &= \frac{3n_6}{m^+}, \\
n_7^+ &= \frac{2n_7}{m^+}, \quad n_7^- = \frac{n_7}{m^-}, \\
n_8^+ &= \frac{n_8}{m^+}, \quad n_8^- = \frac{2n_8}{m^-}, \\
n_9^- &= \frac{3n_9}{m^-}.
\end{aligned}
$$

Note that $n_k^\sigma = 0$ for combinations of k and σ that are not presented above. Both the focal-link and focal-triad models are described by the notations introduced above. When described by rate equations, these two models differ only in their transition probabilities.

Let $p_\sigma^{\sigma'}$ denote the probability that a link changes its sign from σ to σ'. In the focal-link model, considering all such circumstances, we can describe the probabilities $p_\sigma^{\sigma'}$ in terms of triad densities. Accounting for all instances where a link σ transition to σ' (i.e., summing all probabilities of the same color in Figure S1), we obtain the full expressions for $p_\sigma^{\sigma'}$ as follows:

$$
\begin{cases}
p_0^+ = n_0\epsilon + n_1\frac{2}{3}\delta + n_3\frac{1}{3}\eta + n_5\frac{1}{3}\eta, \\
p_0^- = n_0\epsilon + n_2\frac{2}{3}\delta + n_4\frac{1}{3}\eta, \\
p_+^0 = n_1\frac{1}{3}(1-2\epsilon) + n_3\frac{2}{3}(1-\delta) + n_4\frac{1}{3}(1-\delta) + n_6(1-\eta) + n_7\frac{2}{3}(1-\eta) + n_8\frac{1}{3}(1-\eta), \\
p_-^0 = n_2\frac{1}{3}(1-2\epsilon) + n_4\frac{1}{3}(1-\delta) + n_5\frac{2}{3}(1-\delta) + n_7\frac{1}{3}(1-\eta) + n_8\frac{2}{3}(1-\eta) + n_9(1-\eta), \\
p_+^- = n_1\frac{1}{3}\epsilon + n_4\frac{1}{3}\delta + n_7\frac{2}{3}\eta, \\
p_-^+ = n_2\frac{1}{3}\epsilon + n_4\frac{1}{3}\delta + n_7\frac{1}{3}\eta + n_9\eta.
\end{cases}
\tag{S1}
$$

Notice that they are all expressed in terms of the triad frequencies n_k.

The focal-triad model also allows for the probabilities $p_\sigma^{\sigma'}$ to be expressed in terms of triad densities; see also Figure 4 in the main text. They are given by

$$
\begin{cases}
p_0^+ = n_0\hat{\epsilon} + \kappa_1\left(\frac{1}{2}n_1 + \frac{1}{2}n_2 + n_3 + n_5\right), \\
p_0^- = n_0\hat{\epsilon} + \kappa_1\left(\frac{1}{2}n_1 + \frac{1}{2}n_2 + n_4\right), \\
p_+^0 = \kappa_2\Big[n_1 + n_3 + \frac{1}{2}n_4 + n_6 + \frac{2}{3}(1-\hat{\eta})n_7 + \frac{1}{3}n_8\Big], \\
p_-^0 = \kappa_2\Big[n_2 + \frac{1}{2}n_4 + n_5 + \frac{1}{3}(1-\hat{\eta})n_7 + \frac{2}{3}n_8 + (1-\hat{\eta})n_9\Big], \\
p_+^- = \hat{\eta}(1-p)n_7, \\
p_-^+ = \hat{\eta}(pn_7 + n_9).
\end{cases}
\tag{S2}
$$

Now that we have obtained both $\{n_k^\sigma\}_{k,\sigma}$ and $\{p_\sigma^{\sigma'}\}_{\sigma\neq\sigma'}$ as functions of n_k, we can derive corresponding rate equations that govern the time evolution of the triad frequencies n_k:

$$
\begin{cases}
\dot{n}_0 = n_1^+ p_+^0 + n_2^- p_-^0 - n_0^0(p_0^+ + p_0^-), \\
\dot{n}_1 = n_0^0 p_0^+ + n_2^- p_-^+ + n_3^+ p_+^0 + n_4^- p_-^0 - n_1^+(p_+^0 + p_+^-) - n_1^0(p_0^+ + p_0^-), \\
\dot{n}_2 = n_0^0 p_0^- + n_1^+ p_+^- + n_4^+ p_+^0 + n_5^- p_-^0 - n_2^-(p_-^0 + p_-^+) - n_2^0(p_0^+ + p_0^-), \\
\dot{n}_3 = n_1^0 p_0^+ + n_4^- p_-^+ + n_6^+ p_+^0 + n_7^- p_-^0 - n_3^+(p_+^0 + p_+^-) - n_3^0(p_0^+ + p_0^-), \\
\dot{n}_4 = n_1^0 p_0^- + n_2^0 p_0^+ + n_3^+ p_+^- + n_5^- p_-^+ + n_7^+ p_+^0 + n_8^- p_-^0 - n_4^-(p_-^0 + p_-^+) - n_4^+(p_+^0 + p_+^-) - n_4^0(p_0^+ + p_0^-), \\
\dot{n}_5 = n_2^0 p_0^- + n_4^+ p_+^- + n_8^+ p_+^0 + n_9^- p_-^0 - n_5^-(p_-^0 + p_-^+) - n_5^0(p_0^+ + p_0^-), \\
\dot{n}_6 = n_3^0 p_0^+ + n_7^- p_-^+ - n_6^+(p_+^0 + p_+^-), \\
\dot{n}_7 = n_3^0 p_0^- + n_4^0 p_0^+ + n_6^+ p_+^- + n_8^- p_-^+ - n_7^-(p_-^0 + p_-^+) - n_7^+(p_+^0 + p_+^-), \\
\dot{n}_8 = n_4^0 p_0^- + n_5^0 p_0^+ + n_7^+ p_+^- + n_9^- p_-^+ - n_8^-(p_-^0 + p_-^+) - n_8^+(p_+^0 + p_+^-), \\
\dot{n}_9 = n_5^0 p_0^- + n_8^+ p_+^- - n_9^-(p_-^0 + p_-^+).
\end{cases}
\tag{S3}
$$

It is worth noting that the above equations are *closed* with respect to the triad frequencies $\{n_k\}_{k=0,\ldots,9}$, making them ready for analysis. To examine whether the rate equations accurately predict the behavior of our stochastic models, we refer the reader to Figure 5 in the main text, which presents results from stochastic simulations alongside mean-field predictions.

Furthermore, it is crucial to understand how parameters influence triad frequencies at equilibrium. Figure S2 shows equilibrium triad frequencies change with ϵ and δ for a fixed η in the focal-link model, and with $\hat{\epsilon}$ and $\hat{\kappa}$ for a fixed $\hat{\eta}$ in the focal-triad model. Likewise, Figure S3 shows equilibrium triad frequencies for different values of δ and η given a fixed ϵ in the focal-link model, and $\hat{\kappa}$ and $\hat{\eta}$ given a fixed $\hat{\epsilon}$ in the focal-triad model. We obtained these numerical results by evolving Eq. S3.

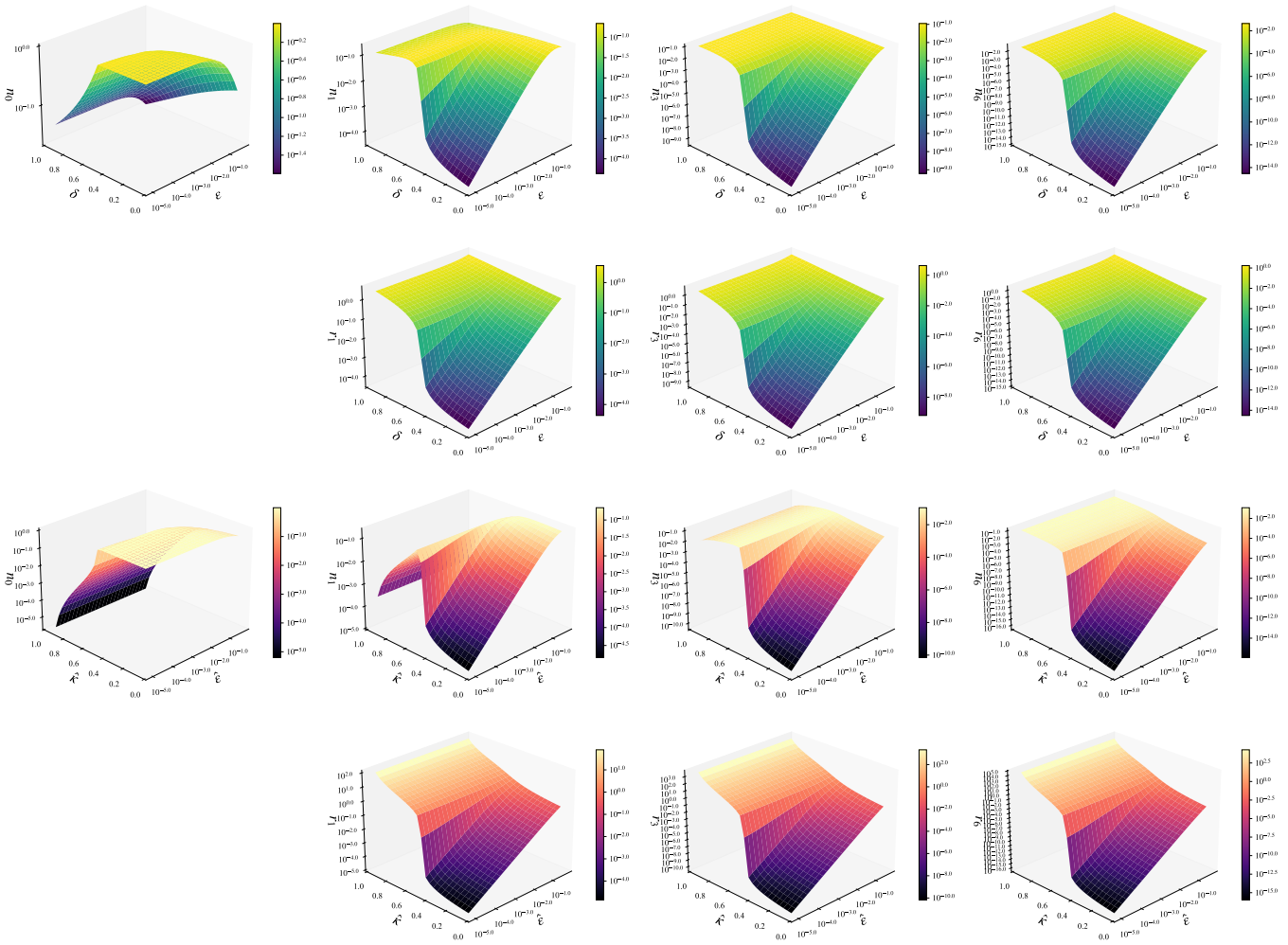

Figure S2. Equilibrium triad frequencies as functions of ϵ and δ (focal-link model) and $\hat{\epsilon}$ and $\hat{\kappa}$ (focal-triad model). We assumed the relation $\kappa_2 = 1 - \kappa_1$ so that $\hat{\kappa} = \kappa_1$. Parameters: $\eta = 0.5$, $\hat{\eta} = 0.5$. Only n_0, n_1, n_3, n_6 and r_1, r_3, r_6 are visualized. We imposed $\delta, \hat{\kappa} \in [0.05, 0.95]$ to avoid numerical instability.

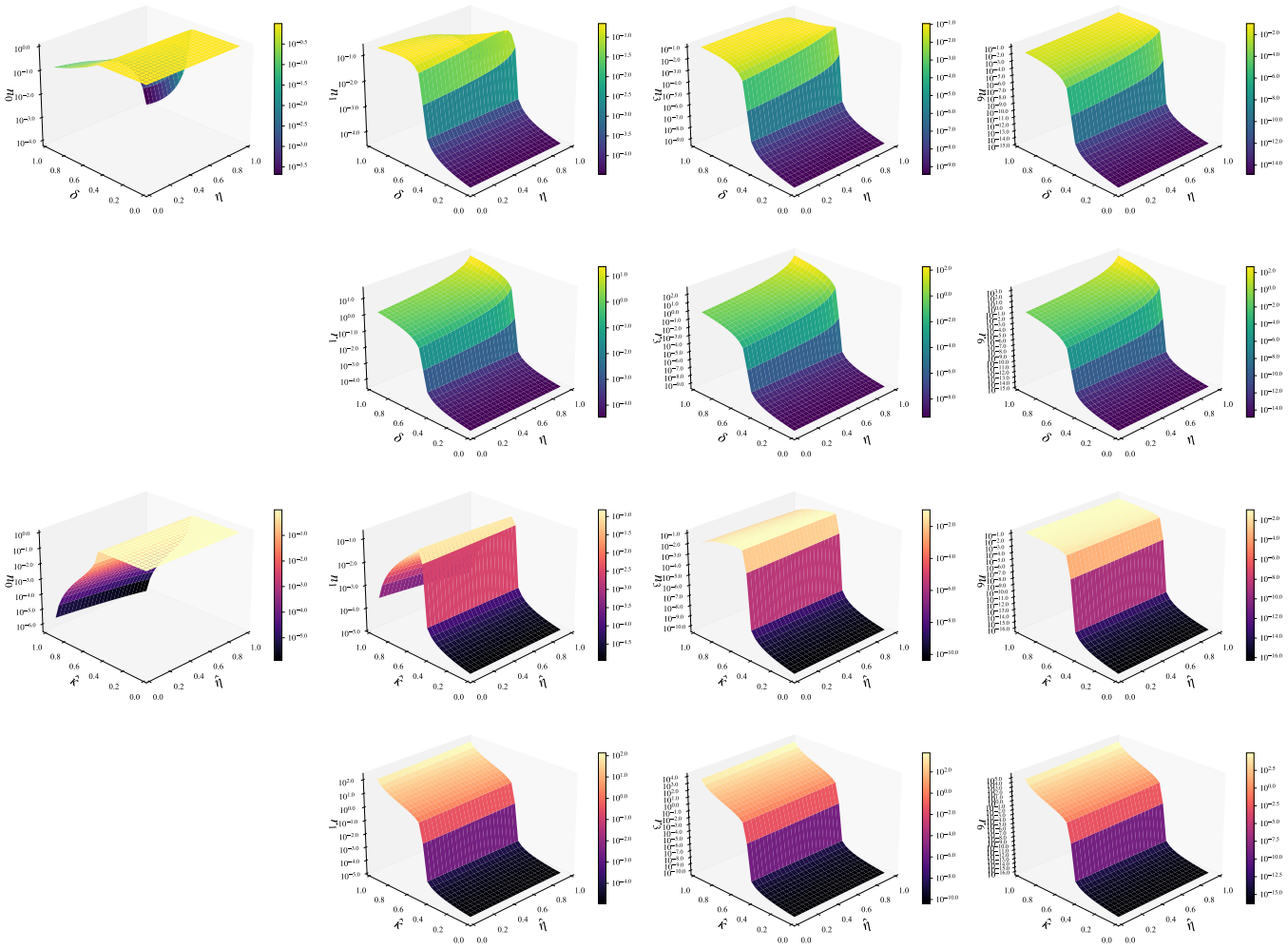

Figure S3. Equilibrium triad frequencies as functions of δ and η (focal-link model); $\hat{\kappa}$ and $\hat{\eta}$ (focal-triad model). We assumed the relation $\kappa_2 = 1 - \kappa_1$ so that $\hat{\kappa} = \kappa_1$. Parameters: $\epsilon = 10^{-5}$, $\hat{\epsilon} = 10^{-5}$, and $\kappa_2 = 0.5$. Only n_0, n_1, n_3, n_6 and r_1, r_3, r_6 are visualized. We imposed $\delta, \eta, \hat{\kappa}, \hat{\eta} \in [0.04, 0.96]$ to avoid numerical instability.

2. EQUILIBRIUM TRIAD FREQUENCIES

In this section, we present a method to obtain approximate equilibrium triad frequencies. As mentioned in the main text, since Eq. S3 consists of ten variables and is highly nonlinear, exact equilibrium solutions are virtually impossible to obtain. To tackle this difficulty, we develop an approximation method that can reduce the complexity of the ODE system systematically and yield approximate equilibrium solutions in a self-consistent way. More specifically, assuming certain parameter conditions, we solve the equations *sequentially*, instead of *simultaneously*, using a hierarchy of the equilibrium triad frequencies and a separation of timescales.

When a system of interacting particles is in equilibrium, some explicit ansatzes are often assumed. As a first step of the reduction, we assume the *activation-limited regime*, i.e., that a majority of links are inactive. In the activation-limited regime, in which the frequencies of bottom-row triads are negligible compared to others, sign symmetry is expected in both link and triad frequencies. More specifically, exchanging positive and negative links does not affect the frequencies of triads that transform into each other. Under this assumption, the following relations hold:

$$n_1 = n_2, \quad n_3 = n_5, \quad n_6 = n_9, \quad n_7 = n_8. \tag{S4}$$

It is easy to see that the relation $\rho^+ = \rho^-$ also holds in this scenario. These assumptions are easily justifiable because when most links are inactive, the bottom-row triad configurations rarely exist, and those above the bottom row in Figure S1 exhibit left-right symmetry in the way that the transition probabilities between different triad types are specified. This also extends to the focal-triad model (see Figure 4 in the main text). In addition, equilibrium sign symmetry with respect to triad frequencies in the activation-limited regime leads to another set of conditions on the probabilities $p_\sigma^{\sigma'}$:

$$p_0^+ = p_0^-, \quad p_+^0 = p_-^0, \quad p_+^- = p_-^+. \tag{S5}$$

Here these equalities arise from the assumption that link and triad frequencies are sign symmetric. Plugging Eqs. S4 and S5 into Eqs. S1 (or S2) yields the following two relations:

$$2n_3 = n_4, \quad 3n_6 = n_7. \tag{S6}$$

We note that Eq. S6 holds in both the focal-link and focal-triad models. In short, within the activation-limited regime, we can significantly reduce the complexity of the system—effectively from a ten-variable to a four-variable ODE system described by only n_0, n_1, n_3, and n_6. We will later show that this method produces self-consistent predictions that are in good agreement with stochastic simulation data, provided that the system is in the activation-limited regime.

Furthermore, when a majority of links are inactive, the frequencies of triad configurations should be in different orders of magnitude, that is,

$$n_0 \gg n_1, n_2 \gg n_3, n_4, n_5 \gg n_6, n_7, n_8, n_9. \tag{S7}$$

The above relation allows us to ignore "higher-order" terms when appropriate. This should also be accompanied by a hierarchy of relaxation times for each variable: that is, n_0 reaches equilibrium faster than n_1 and n_2; n_1 and n_2 reach equilibrium faster than n_3, n_4, and n_5; and n_3, n_4, and n_5 reach equilibrium faster than n_6, n_7, n_8 and n_9. This timescale separation allows for certain variables to be eliminated sequentially. Therefore, we can approximately find the steady state of the rate equations (Eq. S3), by solving them one by one, from top to bottom.

3. FOCAL-LINK MODEL: APPROXIMATE STEADY-STATE SOLUTION

We set out to compute approximate equilibrium solutions in the activation-limited regime, using the conditions mentioned earlier. For convenience, we introduce the rescaled frequency r_k, define by

$$r_k = \frac{n_k}{n_0}, \quad k = 1, \cdots, 9. \tag{S8}$$

3.1. Approximate equilibrium frequency of Δ_1 triads

By setting $\dot{n}_0 = 0$ in Eq. S3, we seek to find an approximate form of r_1. Applying Eqs. S4 and S6, we find

$$n_1 p_+^0 m^0 = 3 n_0 p_0^+ m^+. \tag{S9}$$

Unpacking the expressions and ignoring higher-order terms using Eq. S7 (i.e., terms with n_k for $k \leq 3$), we find that the following quadratic equation holds approximately:

$$4(1-2\epsilon) r_1^2 + 3(1-2\epsilon-2\delta) r_1 - 9\epsilon = 0. \tag{S10}$$

Given $r_1 > 0$, we obtain

$$r_1 \simeq \frac{6\epsilon}{(1-2\epsilon-2\delta) + \sqrt{(1-2\epsilon-2\delta)^2 + 16(1-2\epsilon)\epsilon}}. \tag{S11}$$

The approximate relation above is valid only when ϵ is small, provided the activation-limited regime. Case in point: r_1 tends to infinity as ϵ approaches $1/2$ from below for any δ, which does not align with the assumption $\dot{n}_0 = 0$.

Equation S11 exhibits several noteworthy characteristics. First, in the small ϵ-limit, the approximate r_1 behaves asymptotically as

$$r_1 \sim \begin{cases} 3\epsilon & \delta \approx 0, \\ \dfrac{3}{2}\sqrt{\epsilon} & \delta = 1/2, \\ \dfrac{3}{4} & \delta \approx 1. \end{cases} \tag{S12}$$

Moreover, we find from Eq. S10 that as ϵ tends to 0, it behaves as

$$r_1 \to \begin{cases} 0 & \delta \leq 1/2, \\ \dfrac{3(2\delta-1)}{4} & \delta \geq 1/2. \end{cases} \tag{S13}$$

As mentioned in the main text, Eq. S13 implies that in the limit $\epsilon \to 0$, a phase transition occurs at $\delta = 1/2$, which we later confirm corresponds to the emergence of a giant component connected by active links. We could naively infer this limiting behavior by simply substituting $\epsilon = 0$ into Eq. S10. However, to formally preclude the trivial solution (i.e., $r_1 = 0$) in the supercritical regime, we should perform a power-series expansion for r_1 when solving Eq. (S10), provided that ϵ is small.

3.2. Derivation of an approximate expression for r_1 using a power-series expansion

We expand r_1 as $r_1 = r_{10} + \epsilon r_{11} + \epsilon^2 r_{12} + \cdots$ for small ϵ. Substituting it into Eq. S10 gives

$$4(1-2\epsilon)(r_{10} + \epsilon r_{11} + \epsilon^2 r_{12} + \cdots)^2 + 3(1-2\epsilon-2\delta)(r_{10} + \epsilon r_{11} + \epsilon^2 r_{12} + \cdots) - 9\epsilon = 0.$$

We then collect terms by powers of ϵ. For $O(1)$, we have

$$4 r_{10}^2 + 3(1-2\delta) r_{10} = 0, \tag{S14}$$

whose solution is

$$r_{10} = 0 \quad \text{or} \quad r_{10} = \frac{3(2\delta-1)}{4}. \tag{S15}$$

For $O(\epsilon)$, we have

$$-8r_{10}^2 + 8r_{10}r_{11} - 6r_{10} + 3(1-2\delta)r_{11} - 9 = 0, \tag{S16}$$

which has the solution

$$r_{11} = \frac{8r_{10}^2 + 6r_{10} + 9}{8r_{10} + 3(1-2\delta)}, \tag{S17}$$

given r_{10}. Depending on the zeroth-order solution, it is

$$r_{11} = \frac{3}{1-2\delta} \quad \text{or} \quad r_{11} = \frac{3(2\delta-1)}{2} + \frac{1}{2} + \frac{3}{2\delta-1}. \tag{S18}$$

Piecing them back together, we find

$$r_1 = \begin{cases} \dfrac{3\epsilon}{1-2\delta} + O(\epsilon^2), & \text{or} \\ \dfrac{3(2\delta-1)}{4} + \left[\dfrac{3(2\delta-1)}{2} + \dfrac{1}{2} + \dfrac{3}{2\delta-1}\right]\epsilon + O(\epsilon^2). \end{cases} \tag{S19}$$

When $\delta < 1/2$, the first solution applies because ϵ is strictly positive and r_1 is nonnegative by construction, which can be confirmed by taking only the leading-order terms into account. Likewise, when $\delta > 1/2$, the second solution applies. Therefore, we conclude that for a fixed δ,

$$r_1 \to \begin{cases} 0 & \delta \le 1/2, \\ \dfrac{3(2\delta-1)}{4} & \delta \ge 1/2, \end{cases}$$

as $\epsilon \to 0^+$. We finally note that Eq. S19 is invalid when $\delta = 1/2$; however, Eq. S11 is sufficient to show that r_1 tends to zero as $\epsilon \to 0^+$ when $\delta = 1/2$.

3.3. Approximate equilibrium frequencies of Δ_3 and Δ_6 triads

Similarly, we set $\dot{n}_1 = 0$ to derive a closed-form equation for r_3. Under the symmetry condition, we find

$$m^+(3n_0 - 4n_1)p_0^+ = m^0(n_1 - 4n_3)p_+^0. \tag{S20}$$

Ignoring higher order terms (i.e., those with n_6) yields

$$\begin{aligned} &64(1-\delta)r_3^3 + \left[16(4 - 2\epsilon - 3\delta - 2\eta) + 24(2 - 2\delta - \eta)\right] r_3^2 \\ &\quad + \left[4(-1 - 4\delta + 6\epsilon - 2\eta)r_1^2 + 6(6\delta - 12\epsilon + \eta)r_1 + 36\epsilon\right] r_3 + \left[4(5\epsilon - 4)r_1^2 + 3(5\epsilon - 1)r_1\right] = 0, \end{aligned} \tag{S21}$$

given r_0. Similarly, we can obtain a closed-form expression for r_6. Setting $\dot{n}_6 = 0$ yields

$$n_3 p_0^+ m^+ = 3n_6 p_+^0 m^0. \tag{S22}$$

Here, we note that there is no term to neglect since there are no remaining terms of orders that are smaller than r_6. Reorganizing the equation above gives the quadratic equation

$$\begin{aligned} &36(1-\eta)(3 + 4r_1 + 4r_3)r_6^2 \\ &\quad + \left[9(1-2\epsilon)r_1 + 12(1-2\epsilon)r_1^2 + 12(5 - 2\epsilon - 6\delta)r_1 r_3 + 36(1 - \epsilon - \delta)r_3 + 24(2 - 2\delta - \eta)r_3^2\right] r_6 \\ &\quad + (r_1 + 4r_3)r_3(3\epsilon + 2r_1\delta + 2r_3\eta) = 0, \end{aligned} \tag{S23}$$

given r_1 and r_3.

We employed symbolic computation to solve these algebraic equations sequentially. The results are presented in Figure S4, which are qualitatively in good agreement with Figure S2 in the activation-limited regime.

Here we show how the rescaled triad densities change with parameters, based on both our mean-field analysis and numerical calculations, specifically focusing on the activation-limited regime. In fact, we obtain surprisingly simple results given the complexity of the analysis. They are summarized as follows: for sufficiently small ϵ,

$$\begin{cases} r_1 = r_2 = O(\epsilon^{\alpha}), & \\ r_3 = r_5 = O(\epsilon^{2\alpha}), & r_4 = O(\epsilon^{2\alpha}), \\ r_6 = r_9 = O(\epsilon^{3\alpha}), & r_7 = r_8 = O(\epsilon^{3\alpha}), \end{cases} \tag{S24}$$

where the exponent α changes as

$$\alpha(\delta) \approx \begin{cases} 1 & \delta \approx 0, \\ 1/2 & \delta \approx 1/2, \\ 0 & \delta \approx 1, \end{cases} \tag{S25}$$

and the value of α drops sharply at $\delta \approx 1/2$. The different powers in the scaling laws for different rows of triads in the diagram (Figure 1 in the main text) ensure that our approximation method works in a self-consistent manner. See also Figure 6 in the main text for details.

4. FOCAL-TRIAD MODEL: APPROXIMATE STEADY-STATE SOLUTION

4.1. Approximate equilibrium frequency of Δ_1 triads

Next, we analyze the focal-triad model using the same approach. It is the probabilities $p_\sigma^{\sigma'}$ that distinguish the focal-link and focal-triad models, allowing the focal-triad model to be analyzed in exactly the same way. Using the same approximation method, we obtain a quadratic equation for r_1 similar to Eq. S10, given by

$$4\kappa_2 r_1^2 + 3(\kappa_2 - \kappa_1) r_1 - 3\hat{\epsilon} = 0, \tag{S26}$$

which has the valid solution

$$r_1 = \frac{6\hat{\epsilon}}{3(\kappa_2 - \kappa_1) + \sqrt{9(\kappa_2 - \kappa_1)^2 + 48\kappa_2\hat{\epsilon}}}. \tag{S27}$$

Notice that Eq. S27 does *not* blow up in the limit $\hat{\epsilon} \to 1/2$, which contrasts the focal-link model (see Eq. S10). This equation also serves as a window into how r_1 depends on parameters. The $\hat{\epsilon}$-scaling is given by

$$r_1 \sim \begin{cases} \hat{\epsilon} & \kappa_1 \approx 0,\ \kappa_2 \approx 1, \\ \dfrac{\sqrt{3}}{2\sqrt{\kappa_2}}\sqrt{\hat{\epsilon}} & \kappa_1 = \kappa_2, \\ \dfrac{3|\kappa_1 - \kappa_2|}{4\kappa_2} & \kappa_1 \approx 1,\ \kappa_2 \approx 0, \end{cases} \tag{S28}$$

which corresponds to Eq. S12 in the focal-link model. Furthermore, a phase transition occurs in the limit $\hat{\epsilon} \to 0$ when $\kappa_1 = \kappa_2$, given that $\kappa_2 \neq 0$. That is,

$$r_1 \to \begin{cases} 0 & \kappa_1 \leq \kappa_2, \\ \dfrac{3(\kappa_1 - \kappa_2)}{4\kappa_2} & \kappa_1 \geq \kappa_2, \end{cases} \tag{S29}$$

which corresponds to Eq. S13 in the focal-link model. This can be obtained more rigorously by performing a power-series expansion on Eq. S26.

4.2. Derivation of an approximate expression for r_1 using an asymptotic expansion

Similar to the focal-triad model, we expand r_1 as $r_1 = r_{10} + \hat{\epsilon} r_{11} + \hat{\epsilon}^2 r_{12} + \cdots$ and substitute it into Eq. S26, which gives

$$4\kappa_2(r_{10} + \hat{\epsilon} r_{11} + \hat{\epsilon}^2 r_{12} + \cdots)^2 + 3(\kappa_2 - \kappa_1)(r_{10} + \hat{\epsilon} r_{11} + \hat{\epsilon}^2 r_{12} + \cdots) - 3\hat{\epsilon} = 0.$$

Collecting terms in powers of $\hat{\epsilon}$, for $O(1)$, we obtain

$$r_{10} = 0 \quad \text{or} \quad r_{10} = \frac{3(\kappa_2 - \kappa_1)}{4\kappa_2}. \tag{S30}$$

For $O(\hat{\epsilon})$, we find, depending on the solution of r_{10},

$$r_{11} = \frac{1}{\kappa_2 - \kappa_1} \quad \text{or} \quad r_{11} = \frac{1}{\kappa_1 - \kappa_2}. \tag{S31}$$

Taken together, these results yield

$$r_1 = \begin{cases} \dfrac{1}{\kappa_2 - \kappa_1}\hat{\epsilon} + O(\hat{\epsilon}^2), & \text{or} \\ \dfrac{3(\kappa_2 - \kappa_1)}{4\kappa_2} + \dfrac{1}{\kappa_1 - \kappa_2}\hat{\epsilon} + O(\hat{\epsilon}^2), \end{cases} \tag{S32}$$

which implies Eq. S29 as $\epsilon \to 0^+$, given that $\kappa_1 \neq \kappa_2$ and $\kappa_2 \neq 0$.

4.3. Approximate equilibrium frequencies of Δ_3 and Δ_6 triads

Setting $\dot{n}_1 = 0$ gives

$$m^+(3n_0 - 4n_1)p_0^+ = m^0(n_1 - 4n_3)p_+^0. \tag{S33}$$

Reorganizing the equation and ignoring higher-order terms, we obtain the following cubic equation in r_3:

$$\begin{aligned} 32\kappa_2 r_3^3 + 8\left[(5\kappa_2 - 4\kappa_1)r_1 + 3(\kappa_2 + \kappa_1)\right] r_3^2 \\ + 2\left[2(-3\kappa_1 + \kappa_2)r_1^2 + (9\kappa_1 + 3\kappa_2 - 8\hat{\epsilon})r_1 + 6\hat{\epsilon}\right] r_3 \\ + \left[-4(\kappa_1 + \kappa_2)r_1^3 + \{3(\kappa_1 - \kappa_2) - 4\hat{\epsilon}\} r_1^2 + 3\hat{\epsilon}r_1\right] = 0. \end{aligned} \tag{S34}$$

Similarly, setting $\dot{n}_6 = 0$ yields

$$n_3 p_0^+ m^+ = 3n_6 p_+^0 m^0. \tag{S35}$$

Ignoring higher-order terms, we obtain the following quadratic equation in r_6:

$$\begin{aligned} 6\kappa_2(3 + 4r_1 + 4r_3)(2 - \hat{\eta})r_6^2 \\ + 3\left[8(\kappa_2 - \kappa_1)r_3^2 + 4(3\kappa_2 - \kappa_1)r_1 r_3 + 2(3\kappa_2 - 2\hat{\epsilon})r_3 + 4\kappa_2 r_1^2 + 3\kappa_2 r_1\right] r_6 \\ - (r_1 + 4r_3)r_3(\hat{\epsilon} + \kappa_1 r_1 + 2\kappa_1 r_3) = 0. \end{aligned} \tag{S36}$$

Solving these equations using symbolic computation, we find that

$$\begin{cases} r_1 = r_2 = O(\hat{\epsilon}^\beta), \\ r_3 = r_5 = O(\hat{\epsilon}^{2\beta}), \quad r_4 = O(\hat{\epsilon}^{2\beta}), \\ r_6 = r_9 = O(\hat{\epsilon}^{3\beta}), \quad r_7 = r_8 = O(\hat{\epsilon}^{3\beta}), \end{cases} \tag{S37}$$

where

$$\beta(\delta) = \begin{cases} 1 & \kappa_1 \ll \kappa_2, \\ 1/3 & \kappa_1 = \kappa_2, \\ 0 & \kappa_1 \gg \kappa_2, \end{cases} \tag{S38}$$

and β changes rapidly around $\kappa_1 = \kappa_2$. See also Figure 6 in the main text.

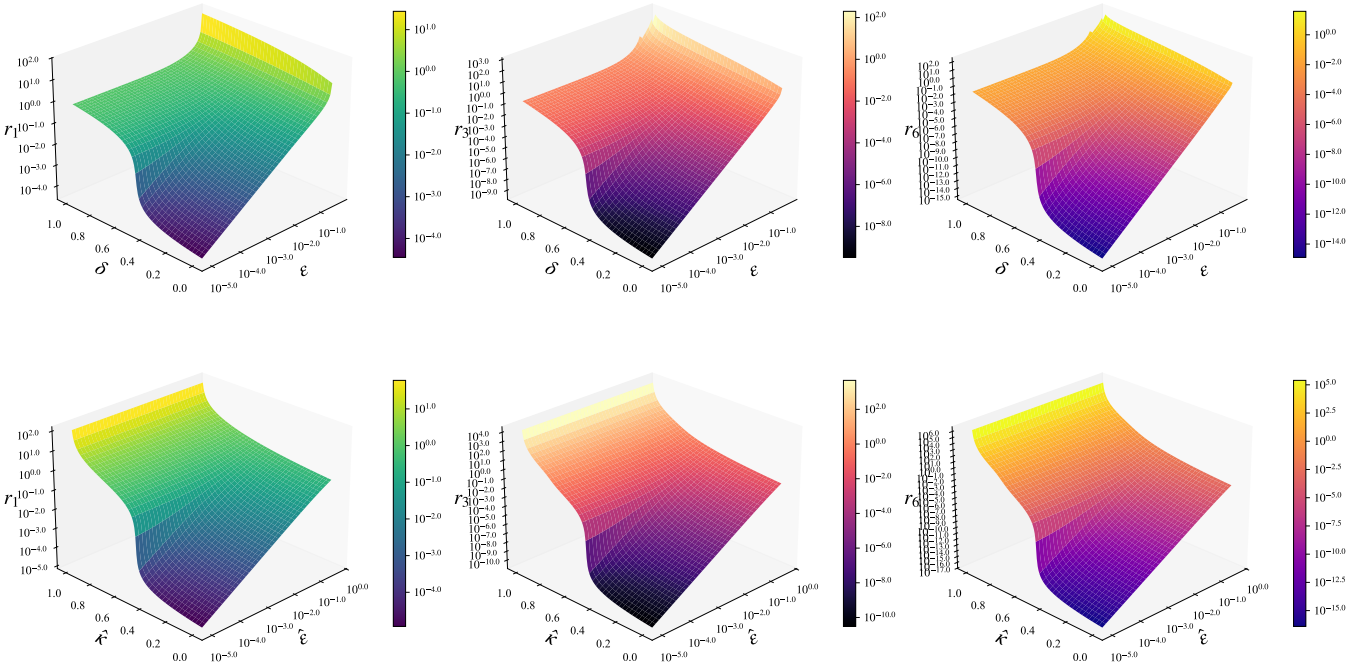

Figure S4. Equilibrium rescaled triad frequencies r_k derived analytically using our approximation method ($k = 1, 3, 6$). The corresponding equations are Eqs. S11, S21, and S23 for the focal-link model (top row panel), and Eqs. S27, S34, and S36 for the focal-triad model (bottom row panel). We used symbolic computation to find r_3 and r_6. Parameters: $\epsilon \in [10^{-5}, 0.49]$, $\delta \in [0, 1], \eta = 0.5$ (focal-link model); $\hat{\epsilon} \in [10^{-5}, 0.5], \hat{\kappa} \in [0, 1], \hat{\eta} = 0.5, \kappa_2 = 1 - \kappa_1$ (focal-triad model).

5. FREQUENCY OF IRRATIONAL UPDATES

In this section, we analyze how frequently irrational updates occur in each model and confirm that the focal-triad model, as intended, substantially reduces the instances of irrational update events—including not only intentional irrational updates but also incidental ones. For the definition of an irrational update and an illustrative example, see Sec. IIA and Figure 3 in the main text. An irrational update is any transition event that is either $\Delta_3 \to \Delta_4$, $\Delta_5 \to \Delta_4$, $\Delta_4 \to \Delta_3$, or $\Delta_4 \to \Delta_5$, whose rate of occurrence is calculated by $p_+^- n_3^+$, $p_-^+ n_5^-$, $p_-^+ n_4^-$, or $p_+^- n_4^+$, respectively. Using Eqs. S1 and S2, we can calculate the average frequency of irrational transition events per unit time, which we denote by I_m $(m = 1, 2)$. In the focal-link model $(m = 1)$, it is given by

$$I_1 = (n_3^+ + n_4^-)\left[\epsilon\frac{1}{3}n_1 + \delta\frac{1}{3}n_4 + \eta\frac{2}{3}n_7\right] + (n_4^- + n_5^-)\left[\epsilon\frac{1}{3}n_2 + \delta\frac{1}{3}n_4 + \eta(\frac{1}{3}n_7 + n_9)\right]. \tag{S39}$$

In the focal-triad model $(m = 2)$, it is given by

$$I_2 = (n_3^+ + n_4^-)\hat{\eta}\frac{2}{3}n_7 + (n_4^- + n_5^-)\hat{\eta}\left(\frac{1}{3}n_7 + n_9\right). \tag{S40}$$

Given the equilibrium triad frequencies n_k, in the subcritical regime (i.e., $\delta < 1/2$ and $\kappa_1 < \kappa_2$) with sufficiently small ϵ and $\hat{\epsilon}$, it is guaranteed that I_1 is substantially larger than I_2 since the bottom-row triads Δ_7, Δ_9 are significantly less frequent than the triad types in the middle two rows $\Delta_3, \Delta_4, \Delta_5$, due to the different orders of magnitude of n_k with respect to ϵ (see Eqs. S24 and S37). On the other hand, in the supercritical regime, in which the bottom-row triads dominate, the difference between I_1 and I_2 diminishes and becomes negligible.

6. TIME-SERIES TRIAD FREQUENCIES WITH FULLY POLARIZED INITIAL STATES

Figure S5 shows how neutrality breaks complete balance in our models with fully polarized initial states. A strongly polarized state, where most triads are balanced, may persist temporarily, but it eventually collapses into a transient regime where balanced triads no longer dominate. These two examples in Figure S5 demonstrate that a slight shift in parameter values can disrupt the initial balance and eventually lead to transient dynamics.

Note that it may not be sufficient to change only one of the parameter values to break the initial complete balance: rather, the parameter values should be varied so that neutral links can emerge with positive probability from a completely balanced state. For example, decreasing $\hat{\eta}$ from 1 *alone* does not break balance in the focal-triad model. These cases are nonetheless negligible in the full parameter space.

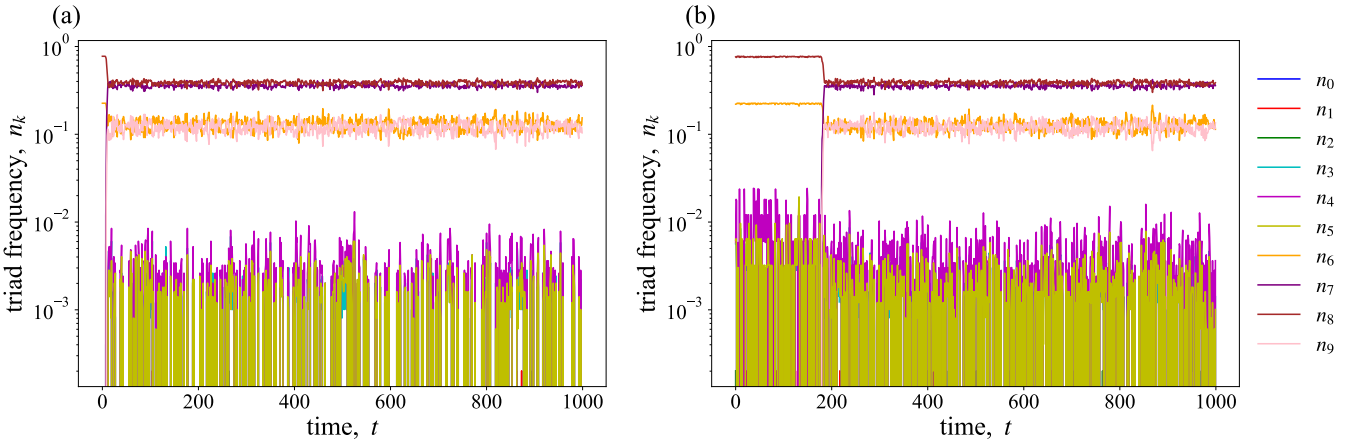

Figure S5. Time-series triad frequencies in (a) the focal-link model and (b) the focal-triad model, with fully polarized initial states. Initially, the population consists of two equally sized factions where links within each faction are positive but links between them are negative, i.e. a fully polarized state. Parameters: $\epsilon = 0.5$, $\delta = 1.0$, $\eta = 0.999$ in the focal-link model, and $\hat{\epsilon} = 0.5$, $\kappa_1 = 0.99$, $\kappa_2 = 0.01$, $\hat{\eta} = 1.0$ in the focal-triad model. The population size is $N = 32$ in both panels.